High order quadratures for the evaluation of interfacial velocities in axi-symmetric Stokes flows

Hector D. Ceniceros

Department of Mathematics, University of California Santa Barbara, CA 93106

Aino L. Karniala

Birkerod Gymnasium and International Baccalaureate School, Sondervangen 56, 3460 Birkerod Denmark

Monika Nitsche *

Department of Mathematics and Statistics, University of New Mexico, Albuquerque, NM 87131

Abstract

Boundary integral methods have been used widely for the simulation of interfacial Stokes flows. These free surface representations reduce the problem to one defined solely on the fluid interface. Often the assumption of axi-symmetry is used to further reduce the dimensionality of the problem. However, it is difficult to obtain high order approximations to the resulting line integrals due to their singular nature and intricate structure. Existing quadrature rules for numerical integration of the interfacial velocity are, at best, of a limited second order accuracy. In this work, we analyze the problem of attaining higher order quadratures and propose new numerical approaches to overcome all the difficulties. These approaches are based on analytic and local error corrections constructed from an asymptotic analysis of the integrands. We present quadratures that achieve a uniform accuracy of up to order five and demonstrate numerically their superior accuracy and efficiency.

Key words: singular integrals, boundary integral methods, complete elliptic integrals.

* Corresponding author

Email addresses: hdc@math.ucsb.edu (Hector D. Ceniceros), ainolk@math.ucsb.edu (Aino L. Karniala), nitsche@math.unm.edu (Monika Nitsche).

1 Introduction

Boundary integral methods have been used extensively to study the motion of single or multiple drops or bubbles in Stokes flows (see e.g. the reviews [1,2] and [3–8]). The basic numerical approach was first described by Youngren and Acrivos [9] and since then significant progress has been made in the extensions of the boundary integral formulation and on the development of more accurate and efficient methods as reviewed by Pozrikidis [10,11]. The boundary integral approach is attractive because it reduces the problem to one defined on the fluid interface only. Under the assumption of axial symmetry the problem is further reduced to a one-dimensional one. This feature makes it possible to achieve, at least in principle, high resolution of interfacial quantities which is necessary for the investigation of the small scale phenomena that occur during coalescence and break-up. Unfortunately, the evaluation of the resulting line integrals that give the interfacial velocity is computationally expensive and standard high order quadratures cannot be applied due to the intricate singular structure of the integrands.

In this work, we analyze the problem of attaining higher order quadratures for axi-symmetric Stokes flow and propose new numerical approaches to achieve this goal. We follow closely the construction of high order quadratures proposed by Nitsche for the case of axi-symmetric, interfacial, Eulerian flows [12]. There are however additional challenges for the Stokes quadratures due to the highly complex structure of the integrands. We perform a detailed asymptotic expansion of the integrands to obtain systematically point-wise corrections to the trapezoidal rule guided by the modified Euler-Maclaurin formula of Sidi and Israeli [13]. Within this framework, we show that the popular "desingularized" (only the leading order singularity is extracted from the integrand) trapezoidal rule [8] is second order accurate uniformly. The asymptotic analysis shows that the leading order desingularization is only advantageous for the single layer potential but there is no apparent gain for the double layer potential.

The asymptotic analysis also reveals that for higher order approximations the coefficients in the expansions are themselves singular at the poles of symmetry and as a consequence the accuracy degrades around that region. To overcome this difficulty and achieve high order accuracy *uniformly* we construct local quadrature corrections around the poles. Unfortunately, high order approximations are quickly overshadowed by round-off errors due to a large cancellation of digits that occurs when evaluating a combination of highly singular terms for the double layer potential. We identify the terms contributing to the large round-off errors and combine them in a suitable way to remedy the problem. The end result is a set of new, uniformly high order quadratures that add little overhead to the commonly used second order approximations and thus can attain a given accuracy for a fraction of the computational cost.

The rest of the paper is organized as follows. In Section 2, we give a brief description of the boundary integral formulation for the motion of one drop in axi-symmetric Stokes flow and introduce the notation we will use for the boundary integral terms. We devote Section 3 to construct point-wise high order quadratures based on a detailed asymptotic analysis of the integrands. The local, pole error corrections are introduced in Section 4 to yield uniformly accurate quadrature formulas. The accuracy and performance of the new quadrature is also demonstrated numerically in Section 4.

2 Governing Equations

2.1 The boundary integral formulation

We consider a drop of fluid with viscosity μ_d surrounded by a fluid of viscosity μ_e and affected by an external flow field $\mathbf{u}^\infty$. Neglecting inertia terms (Stokes flow) and assuming constant surface tension σ, the velocity components u_j at a point $\mathbf{x_0}$ on the surface S of the drop can be written in the following boundary integral representation [10]:

$$u_j(\mathbf{x_0}) = \frac{2}{1+\lambda}\, u_j^\infty(\mathbf{x_0}) - \frac{1}{\mu_e(1+\lambda)} u_j^s(\mathbf{x_0}) + \sigma\frac{1-\lambda}{1+\lambda} u_j^d(\mathbf{x_0}), \tag{1}$$

for $j = 1, 2, 3$, where $\lambda = \mu_d/\mu_e$ and u^s and u^d are the single and double layer boundary integral contributions to the interfacial velocity, respectively, and are given by

$$u_j^s(\mathbf{x_0}) = \frac{1}{4\pi}\int_S G_{ij}(\mathbf{x},\mathbf{x_0}) n_i(\mathbf{x})\kappa(\mathbf{x}) dS(\mathbf{x}), \tag{2}$$

$$u_j^d(\mathbf{x_0}) = \frac{1}{4\pi}\int_S u_i(\mathbf{x}) T_{ijk}(\mathbf{x},\mathbf{x_0}) n_k(\mathbf{x}) dS(\mathbf{x}), \tag{3}$$

for $j = 1, 2, 3$. Here κ is the *total* curvature and G_{ij} is the Stokeslet tensor (free space Green's function):

$$G_{ij}(\mathbf{x},\mathbf{x_0}) = \frac{\delta_{ij}}{r} + \frac{(x_i - x_{0i})(x_j - x_{0j})}{r^3}, \tag{4}$$

where δ_{ij} is the Kronecker delta and $r = \|\mathbf{x} - \mathbf{x_0}\|$. T_{ijk} is the associated stress tensor

$$T_{ijk}(\mathbf{x},\mathbf{x_0}) = -6\frac{(x_i - x_{0i})(x_j - x_{0j})(x_k - x_{0k})}{r^5}. \tag{5}$$

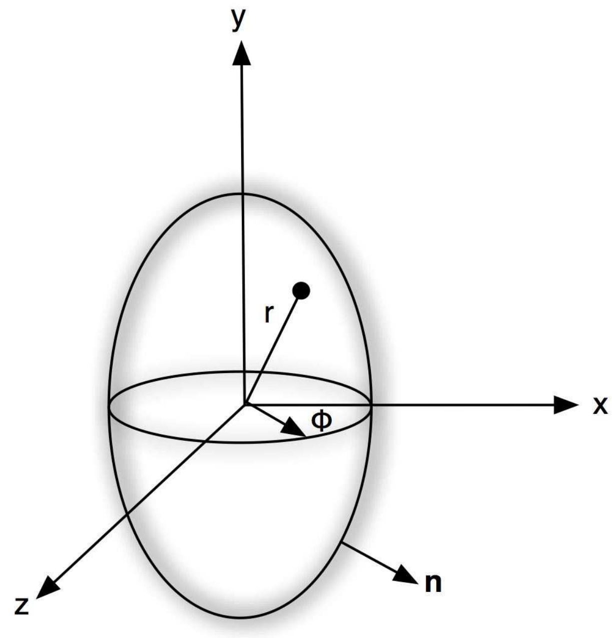

Fig. 1. An axisymmetric drop.

The components of the *outward* unit normal $\mathbf{n}$ are denoted by n_i (n_k) and the summation convention over repeated indices is used. Selecting the radius R of the initial drop as the characteristic length, σ/μ_e as the characteristic velocity, and $R\mu_e/\sigma$ as the characteristic time (1) can be written in dimensionless form as:

$$u_j(\mathbf{x_0}) = \frac{2Ca}{1+\lambda}\, u_j^{\infty}(\mathbf{x_0}) - \frac{1}{1+\lambda} u_j^{s}(\mathbf{x_0}) + \frac{1-\lambda}{1+\lambda} u_j^{d}(\mathbf{x_0}), \tag{6}$$

for $j = 1, 2, 3$, where Ca is a capillary number that measures viscous forces relative to surface tension forces. More specifically, $Ca = \mu_e GR/\sigma$, where G is the magnitude of the rate of strain of the external field $\mathbf{u}^{\infty}$.

In this work we focus on flows with axial symmetry about the y-axis and no swirl (Figure 1). In this special case, the integration with respect to the angular variable ϕ can be performed to reduce the boundary integrals (2) and (3) to line integrals on the trace C of the drop. Because of the symmetry, C can be taken to be the curve defined by the intersection of S with the x-y plane, for $x \geq 0$. The details of the derivation are provided in [10].

The interface C at time t is described in parametric form by $(x(\alpha, t), y(\alpha, t))$ for $0 \leq \alpha \leq \pi$, where $\alpha = 0, \pi$ correspond to the poles, that is, the points at which the interface crosses the axis. The two nonzero velocity components (6) at a point $(x(\alpha_j, t), y(\alpha_j, t))$ are denoted by $u(\alpha_j, t)$ and $v(\alpha_j, t)$ and are given by

$$u(\alpha_j,t) = \frac{1}{1+\lambda}\Big[2Ca\, u_\infty(\alpha_j,t) + u^s(\alpha_j,t) + (1-\lambda)u^d(\alpha_j,t)\Big], \tag{7}$$

$$v(\alpha_j,t) = \frac{1}{1+\lambda}\Big[2Ca\, v_\infty(\alpha_j,t) + v^s(\alpha_j,t) + (1-\lambda)v^d(\alpha_j,t)\Big]. \tag{8}$$

The single and double layer contributions are given by:

$$u^s(\alpha_j,t) = -\frac{1}{4\pi} ⨍_0^\pi H^{us}(\alpha,\alpha_j,t)\kappa(\alpha,t)d\alpha, \tag{9}$$

$$v^s(\alpha_j,t) = -\frac{1}{4\pi} ⨍_0^\pi H^{vs}(\alpha,\alpha_j,t)\kappa(\alpha,t)d\alpha, \tag{10}$$

$$u^d(\alpha_j,t) = \frac{1}{4\pi}\int_0^\pi H_1^{ud}(\alpha,\alpha_j,t)u(\alpha,t) + H_2^{ud}(\alpha,\alpha_j,t)v(\alpha,t)d\alpha, \tag{11}$$

$$v^d(\alpha_j,t) = \frac{1}{4\pi}\int_0^\pi H_1^{vd}(\alpha,\alpha_j,t)u(\alpha,t) + H_2^{vd}(\alpha,\alpha_j,t)v(\alpha,t)d\alpha, \tag{12}$$

where $⨍$ stands for Cauchy's principal value integral and the functions H are given by

$$H^s(\alpha,\alpha_j,t) = M_1(x,x_j,y-y_j)\dot{y}(\alpha,t) - M_2(x,x_j,y-y_j)\dot{x}(\alpha,t), \tag{13}$$

and

$$H_j^d(\alpha,\alpha_j,t) = Q_{j1}(x,x_j,y-y_j)\dot{y}(\alpha,t) - Q_{j2}(x,x_j,y-y_j)\dot{x}(\alpha,t), \tag{14}$$

for $j = 1,2$. Here $x = x(\alpha,t), y = y(\alpha,t), x_j = x(\alpha_j,t), y_j = y(\alpha_j,t)$ and the dot stands for differentiation with respect to α. In (13) and (14), and througout the rest of this paper, the absence of superscript u, v implies that it holds for both the u and the v components. The functions M and Q in each case depend in an intricate way on the complete elliptic integrals of the first and second kind and are provided in [10]. We list them in Appendix A in a form that we find more convenient to our purposes.

Finally, the curvature κ is given by

$$\kappa = \frac{\dot{y}}{x\sqrt{\dot{x}^2+\dot{y}^2}} + \frac{\dot{x}\ddot{y}-\dot{y}\ddot{x}}{(\dot{x}^2+\dot{y}^2)^{3/2}}. \tag{15}$$

2.2 The integrands

Each of the integrands in (9)-(12) is a function of α, α_j, and t and we will denote generically as $G(\alpha,\alpha_j,t)$. These functions are singular or weakly singular at $\alpha = \alpha_j$. Using expansions of the complete elliptic integrals about $\alpha = \alpha_j$, one can show that for $\alpha_j \neq 0, \pi$, the integrands are of the form

$$G(\alpha, \alpha_j, t) = \tilde{G}(\alpha, \alpha_j, t) + \sum_{k=k_0}^{\infty} c_k(\alpha_j, t)\ (\alpha - \alpha_j)^k \log|\alpha - \alpha_j|, \tag{16}$$

where $\tilde{G}$ is smooth. For the single layer, $k_0 = 0$ and thus the integrand is unbounded at $\alpha = \alpha_j$. Hence the integrals (9)-(10) have to be understood as principal values. The double layer is slightly more regular with $k_0 = 1$.

We employ this asymptotic behavior of the integrands and the modified Euler-Maclaurin formula of Sidi and Israeli [13] as the central building principle for the high order quadrature rules we propose in this work.

In the limit $\alpha_j \to 0, \pi$, yielding the velocities at poles of symmetry, the integrands simplify and are smooth. That is, they are of the form (16) with $c_k = 0$ for all k. The limiting integrands corresponding to $\alpha_j = 0, \pi$ are stated in Appendix B. The modified trapezoidal rules can be applied to integrate them to desired accuracy with no further complications, and we do not further discuss this case.

2.3 Leading order desingularization

A commonly used approach [11] to evaluate the single layer velocity components u^s and v^s is to employ the flow identity

$$⨍_0^{\pi} H^s(\alpha, \alpha_j, t) d\alpha = 0, \tag{17}$$

which is a restatement of the condition of incompressibility [10], and rewrite

$$u^s = -\frac{1}{4\pi} ⨍_0^{\pi} H^{us}(\alpha, \alpha_j, t)[\kappa(\alpha, t) - \kappa(\alpha_j, t)] d\alpha, \tag{18}$$

$$v^s = -\frac{1}{4\pi} ⨍_0^{\pi} H^{vs}(\alpha, \alpha_j, t)[\kappa(\alpha, t) - \kappa(\alpha_j, t)] d\alpha. \tag{19}$$

This eliminates the leading order singular term $\log|\alpha - \alpha_j|$ and thus the integrands in (18)-(19) are less less singular than those in (9)-(10). It is important to note however that this procedure only weakens the singularity but does not remove it. Indeed, the integrands in (18)-(19) are of the form (16) with $k_0 = 1$ instead of $k_0 = 0$.

The use of (18)-(19) simplifies somewhat the implementation of the quadratures rules we propose here. But more significantly, the new integrands have less singular behavior *at the poles*. This will be described next in Section 3.3.

A similar procedure has been used [8] for the double layer components. It is possible to use another flow identity [10] to rewrite.

$$\begin{aligned} u^d = \fint_0^\pi &[H_1^d(\alpha,\alpha_j,t)u(\alpha,t) - H_1^{d'}(\alpha,\alpha_j,t)u(\alpha_j,t)]\; d\alpha + u(\alpha_j,t) \\ &+ [H_2^d(\alpha,\alpha_j,t)v(\alpha,t) - H_2'^d(\alpha,\alpha_j,t)v(\alpha_j,t)]\; d\alpha, \end{aligned} \tag{20}$$

and similarly for v^d. However, due to the orientational dependence of the integrand, $H \neq H'$ as noted by Davis [8]. Thus, the new integrands are no less singular than the original ones which are bounded and as a result no gain is achieved using this formulation for the construction of our quadratures. Hence, in this work we extract the leading order singular term in the single layer, by employing (18)-(19), but not so for the double layer. The resulting integrands in each case, denoted by G througout the rest of this paper, are given by

$$G_s(\alpha,\alpha_j,t) = H_s(\alpha,\alpha_j,t)[\kappa(\alpha,t) - \kappa(\alpha_j,t)], \tag{21}$$
$$G_d(\alpha,\alpha_j,t) = H_d^1(\alpha,\alpha_j,t)u(\alpha,t) + H_d^2(\alpha,\alpha_j,t)v(\alpha,t). \tag{22}$$

3 Pointwise 5th order approximation

3.1 The approximation

Functions of the form (16) can be integrated to arbitrarily high order using the modified Euler-Maclaurin formula of Sidi and Israeli [13]. The 5th order rule of interest here is:

$$\fint_a^b G(\alpha,\alpha_j,t)d\alpha = T[G]^h_{[a,b]} + O(h^5), \tag{23}$$

where

$$\begin{aligned} T[G]^h_{[a,b]} = h{\sum_{k\neq j}}'' G(\alpha_k,\alpha_j,t) + h\tilde{G}(\alpha_j,\alpha_j,t) + c_0(\alpha_j,t)h\log\frac{h}{2\pi} \\ + \nu_2 c_2(\alpha_j,t)h^3 + \sum_{\substack{k=1\\ k\ odd}}^{3} \gamma_k\Big[\frac{\partial^k G}{\partial\alpha^k}(\pi,\alpha_j,t) - \frac{\partial^k G}{\partial\alpha^k}(0,\alpha_j,t)\Big]h^{k+1}\ . \end{aligned} \tag{24}$$

Here $\alpha_j = a + jh$ is a uniform partition of $[a,b]$ of meshsize h. The double prime on the summation indicates that the first and last summands are weighted by

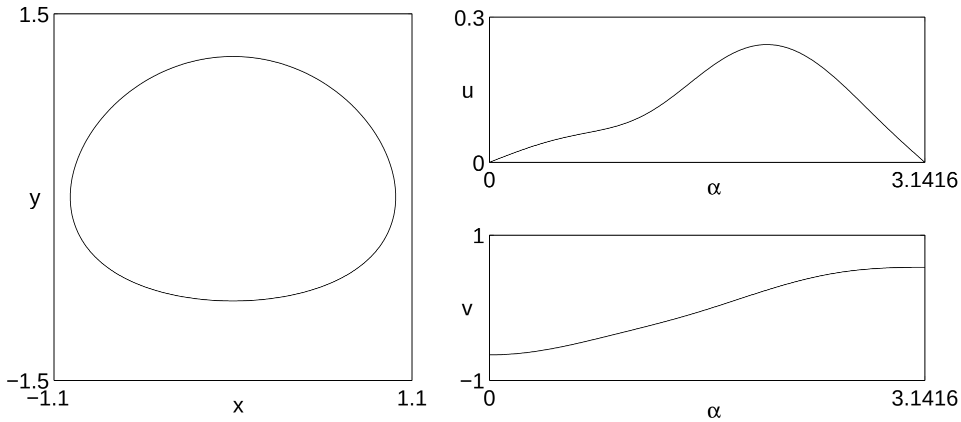

Fig. 2. (a) Position of sheet in x-y plane for the test case. (b) velocity component u and (c) velocity component v.

1/2. The constants appearing in (24) are $\gamma_1 = -1/12$, $\gamma_3 = 1/720$, and $\nu_2 = -0.06089691411678654156....$ Note that for all of our integrands, $c_0(\alpha_j, t) \equiv 0$. Throughout this paper, the approximation error is denoted by

$$E[G]^h_{[a,b]} = \fint_a^b G(\alpha, \alpha_j, t) d\alpha. - T[G]^h_{[a,b]} \tag{25}$$

As shown in [13], $E[G]^h_{[a,b]}$ is of the form

$$\begin{aligned} E[G]^h_{[a,b]} = & \sum_{\substack{k=4 \\ k\ even}}^{m} \nu_k c_k h^{k+1} + \sum_{\substack{k=5 \\ k\ odd}}^{m} \gamma_k \Big[\frac{\partial^k G}{\partial \alpha^k}(\pi, \alpha_j, t) - \frac{\partial^k G}{\partial \alpha^k}(0, \alpha_j, t)\Big] h^{k+1} \\ & + O(h^{m+1}). \end{aligned} \tag{26}$$

for any integer $m \geq 4$.

To test the quadrature (24) we consider the interface at a fixed time, taken to be $t = 0$, and employ

$$x(\alpha, 0) = \sin(\alpha), \tag{27}$$
$$y(\alpha, 0) = -\cos(\alpha) + \epsilon \cos^2(\alpha), \tag{28}$$

with $\epsilon = 0.15$. The interface profile in the x-y plane is shown in Fig 2a. The velocities induced from this profile and for $\lambda = 0$ are displayed in Fig 2bc.

Unless $\lambda = 1$, the double layer contribution turns (7)-(8) into a coupled system of integral equations for the velocity components. This system can be solved efficiently with fixed point iteration and here we do this for $\lambda = 0$. To more clearly separate the contributions to the error arising from the integration of G^s and from that of G^d, we also integrate G^d using a fixed (u, v) in (11)-(12). Specifically, we set $u = \sin\alpha$, $v = \cos\alpha$.

All the coefficients c_k of the integrands G, their values $\widetilde{G}(\alpha_j, \alpha_j, 0)$, and their derivatives at the endpoints, necessary to implement (24), are given in Appendix C. The required derivatives of x, y and κ at $\alpha = \alpha_j, 0, \pi$ are computed spectrally. The quadrature rule (24) is applied using $h = \pi/n$, $n = 32, 64, 128, 256, 512, 1024, 2048$. The integration error is approximated by

$$E[G]^h_{[0,\pi]} \approx T[G]^{\pi/2048}_{[0,\pi]} - T[G]^h_{[0,\pi]}. \tag{29}$$

Figure 3 plots the approximation error for G^{us}, G^{vs}, G^{ud}, G^{vd}. As corresponds to a 5th order quadrature rule, for any fixed value of α_j, the errors decrease as h^5 until roundoff error dominates the results. Note that even though in Fig. 3f there is no sign of a large roundoff error, the accuracy deteriorates for $n \geq 256$. The apparently smooth error in Fig. 3f is somewhat surprising but not so the loss of accuracy as the velocity components are coupled.

It is evident in Fig. 3 that there are two serious problems:

(1) The presence of a large noise due to amplification of roundoff errors.
(2) A loss of accuracy near the poles $\alpha_j = 0, \pi$.

We discuss next how to overcome these problems.

3.2 Controlling roundoff error

While the noise introduced by roundoff error is below 10^{-14} for the single layer integrals [Fig. 3(a)(b)], it is unacceptably large, of the order of 10^{-6} and 10^{-9}, for the double layer integrals [Fig. 3(c)(e)]. In this section we analyze this problem and propose a method for overcoming it.

We note that this large roundoff error is not caused by an inaccurate evaluation of the complete elliptic integrals, $F(k)$ and $E(k)$ in Appendix A, as $k \to 1$ ($\alpha = \alpha_j$) or for $k \to 0$. The latter could be easily remedied by using expansions for $F(k)$ and $E(k)$ to the desired order [14]. As we will see, the large roundoff error is a result of delicate linear combinations of very singular terms.

To find the source of amplification of the roundoff error we have to look closely at the intricate, singular structure of G^{ud} and G^{vd}. We refer to the functions listed in Appendix A for this purpose.

G^{ud} and G^{vd} are functions of Q_{ik}'s. The functions Q_{ik}'s in turn, are a sum of terms proportional to the integrals I_{5j}. For example,

$$Q^u_{11} = -6x[x^3 I_{51} - x^2 x_j (I_{50} + 2I_{52}) + x x_j^2 (I_{53} + 2I_{51}) - x_j^3 I_{52}]. \tag{30}$$

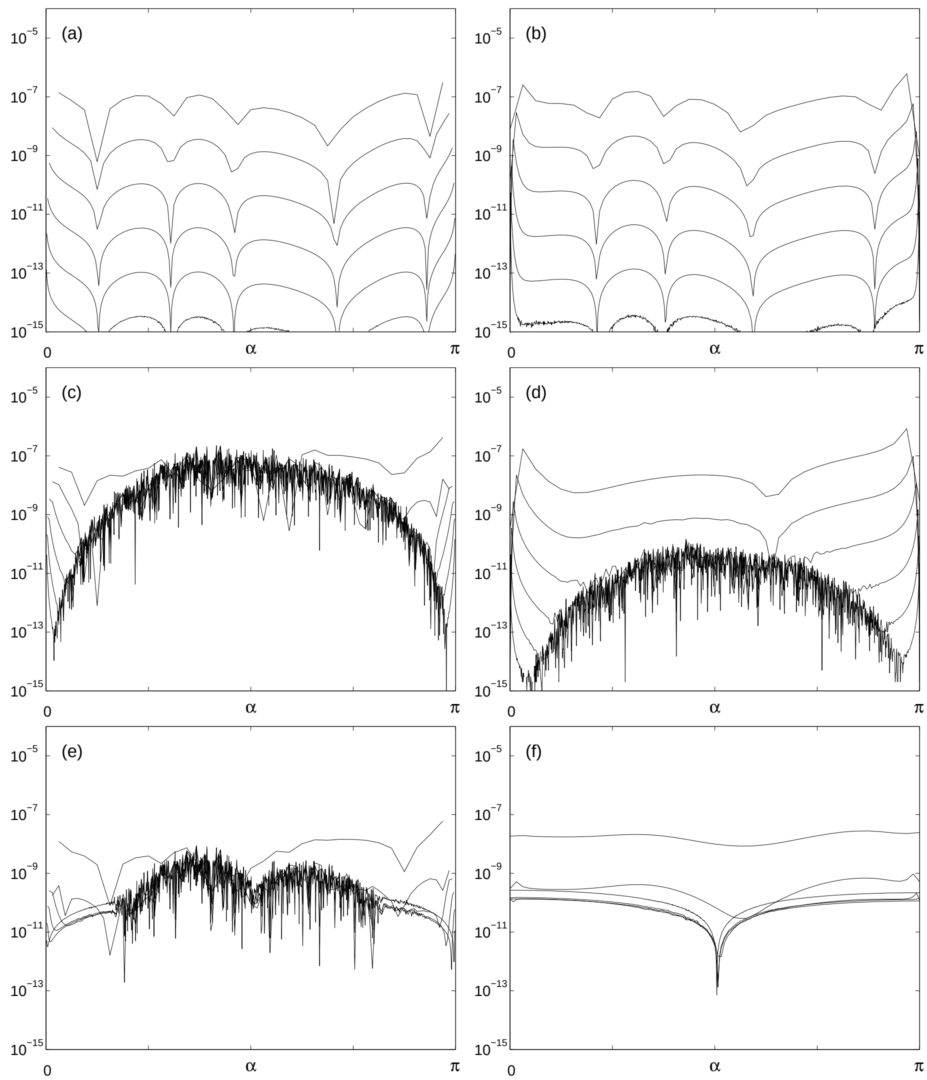

Fig. 3. Approximation error $E[G]^h_{[0,\pi]}$ using different values of $h = \pi/n$, $n = 32$, 64, 128, 256, 512, 1024, for G equal to: (a) and (b) G^{us} and G^{vs}, respectively, (c) and (d) G^{ud} and G^{vd}, respectively, replacing u, v by $\sin\alpha, \cos\alpha$. and (e) and (f) G^{ud} and G^{vd}, with u, v for $\lambda = 0$ obtained iteratively.

The Q's and the I's are singular at $\alpha = \alpha_j$, equivalently, at $x = x_j$ or $k = 1$, where k is as defined in Eq. (A.23). As noted in Appendix A,

$$I_{5j} \sim \frac{1}{x_j^4} \frac{2}{3(1-k^2)^2} = F_{sing} \text{ as } k \to 1. \tag{31}$$

However the Q's are less singular with

$$Q_{ik} \sim \frac{1}{(1-k^2)} \text{ as } k \to 1. \tag{32}$$

This shows that analytically the large singular components in Q_{ik} cancel by subtraction. Performing this operation in finite machine precision leads to large loss of digits of accuracy and a consequently large roundoff error.

To remedy this problem, we extract the singular component from I and compute

$$I'_{ij} = I_{ij} - F_{sing}. \tag{33}$$

This is done by first removing the singular component from $E_{5/2}$:

$$E'_{5/2} = E_{5/2} - \frac{2}{3(1-k^2)^2} \tag{34}$$

and then writing

$$I'_{50} = \frac{4}{c^5} E'_{5/2}, \tag{35}$$

$$I'_{51} = \frac{4}{c^5} a[bE'_{5/2}(k) - E_{3/2}(k)] + \frac{8}{3(1-k^2)k^4}, \tag{36}$$

etc. The functions Q_{ik}'s are then computed by replacing the I_{jk} by I'_{jk}. For example, Q_{11} is computed as follows:

$$\begin{aligned} Q^u_{11} = -6x[x^3 I'_{51} - x^2 x_j (I'_{50} + 2I'_{52}) + x x_j^2 (I'_{53} + 2I'_{51}) - x_j^3 I'_{52} \\ + (x - x_j)^3 F_{sing}], \end{aligned} \tag{37}$$

and similarly for the other Q_{ik}'s.

The reduction in roundoff error is thus obtained by replacing $x^3 - 3x^2 x_j + 3x x_j^2 - x_j^3$ by $(x - x_j)^3$. The result is shown in Fig. 4. The roundoff error noise has been reduced to $O(10^{-13})$. While the noise is still larger than that in the single layer integrals, it is sufficiently low for the method to be used in practical applications that require high accuracy.

3.3 Maximum Error near Poles

For every fixed value of α_j, the error is $O(h^5)$, as shown by the modified Euler-Maclaurin formula of Sidi and Israeli [13]. However, it is evident from Fig. 4 that the error deteriorates near the poles, $\alpha = 0, \pi$, and indeed, the maximum error over all α_j is not $O(h^5)$. That is, the error is pointwise 5th order, but not uniformly over α_j. This is demonstrated in Fig. 8 where we plot the maximum error as a function of h. The figure displays the computed errors for $h = \pi/n$, $n = 32, 64, 128, 256, 512, 1024$ ($\times$) and a line with an indicated slope. Figures (a-d) indicate that the maximum error is $O(h^4)$ for $G^{u,s}$, $O(h^3)$ for $G^{v,d}$ and $G^{v,s}$, and $O(h^2)$ for $G^{u,d}$, assuming u, v is known accurately in G^d. Figures (e-f) show that after solving for u, v iteratively, the $O(h^2)$ errors dominate. Under time evolution, the maximum error will contaminate the solution at all interior points as well, and the 5th order of accuracy is lost. Due to the

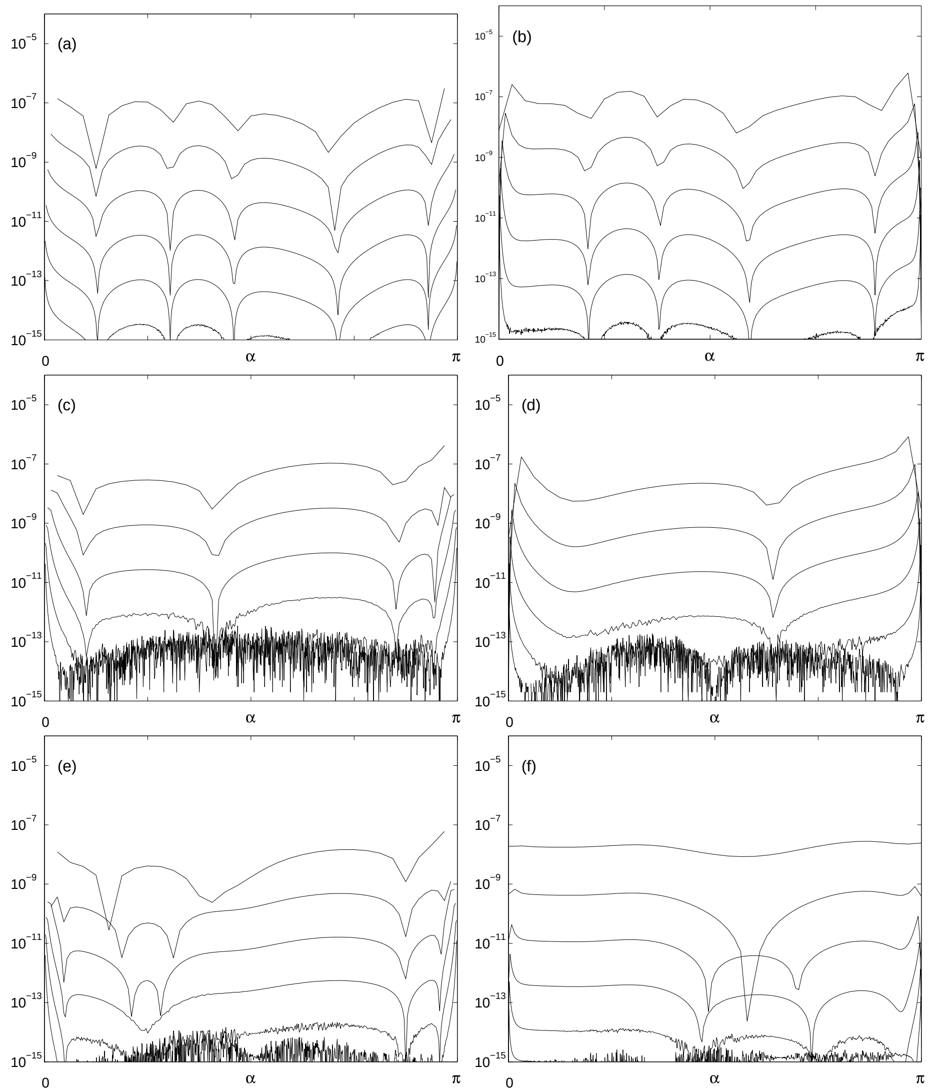

Fig. 4. Approximation error $E[G]^h_{[0,\pi]}$ using the pointwise 5th order method, after correcting for the roundoff error. The values of h are $h = \pi/n$ with $n = 32$, 64, 128, 256, 512, 1024, for G equal to: (a) and (b) G^{us} and G^{vs}, respectively, (c) and (d) G^{ud} and G^{vd}, respectively, replacing u, v by $\sin\alpha, \cos\alpha$. and (e) and (f) G^{ud} and G^{vd}, with u, v for $\lambda = 0$ obtained iteratively.

coupling of the velocity components, the overall accuracy can only be expected to be $O(h^2)$ in a dynamic simulation.

This degeneration of the error near the poles is similar to the one observed for axisymmetric vortex sheets in Eulerian [15–18,12] and Darcian flows [19]. It is caused by the unbounded behaviour of the derivatives of the integrands at the endpoints and the coefficients c_k, as functions of α_j. For example, from the results in the following section and arguments similar to those in [12], one can show that

$$c_k^{ud} \sim \frac{1}{\alpha_j^{k-1}}, \quad \text{as } \alpha_j \to 0. \tag{38}$$

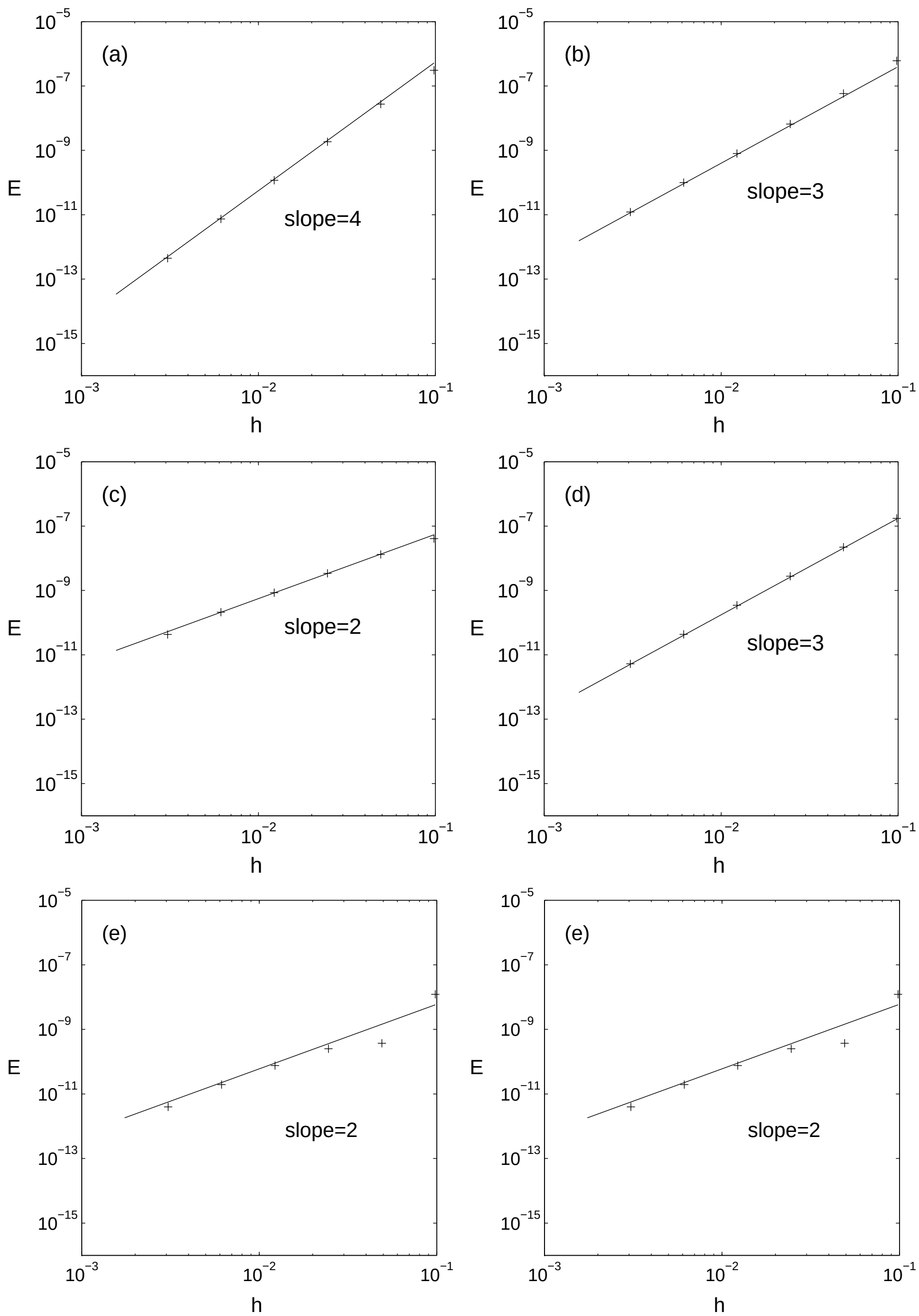

Fig. 5. Maximal Approximation error $\max_{\alpha_j \in [0,\pi/2]} \left(E[G]^h_{[0,\pi]}(\alpha_j) \right)$ using pointwise 5th order method for G equal to: (a) and (b), G^{us} and G^{vs}, respectively. (c) and (d), G^{ud} and G^{vd}, respectively, replacing u, v by $\sin\alpha, \cos\alpha$. (e) and (f), G^{ud} and G^{vd}, respectively, with u, v for $\lambda = 0$ obtained iteratively. The data is shown by $\times$, and the slope of the plotted lines indicates the estimated order of the approximation.

Substituting this expression into (24) and (26) for $\alpha_j = h$ it is clear that the term $c_2 h^3$ as well as all terms involving c_k in the error $E[G^{ud}]$ are of order $O(h^2)$.

The main goal of this paper is to obtain a uniformly accurate 5th order approximation for the integrals of G. We can achieve this by doing a local pole correction to our proposed quadrature (24) using the ideas developed in [12] for inertial vortex sheets.

We remark that without the leading order desingularization (18)-(19) of $G^{u,s}$ and $G^{v,s}$ the behaviour at the poles would be $O(h)$ and $O(h^2)$ respectively, more singular than the one shown in Fig. 4. Thus, the simple trapezoidal rule employed for many years in boundary integral computations of Stokes flows [8,11], requires the leading order desingularization of the single layer integrands to yield uniformly second order results. This "desingularization" extracts the leading order singular term but more importantly smoothes the behaviour of the coefficients at the poles.

4 Uniformly 5th order approximation

Following [12], to obtain a uniformly 5th order quadrature rule we need to capture the singular behaviour of the integrands at the endpoints. We construct first approximations B to the integrands G at the poles using Taylor series expansions. The main idea is to approximate $\int (G - B) d\alpha$ instead of $\int G d\alpha$ using the quadrature rule (24). The approximation of $\int (G - B) d\alpha$ is more accurate at the poles since $G - B$ is less singular there than G, and $\int B d\alpha$ can be computed at minimal cost per timestep, as explained next.

For the left endpoint we use Taylor series about $\alpha, \alpha_j \approx 0$. The symmetry of the interface across the axis implies that the functions $x(\alpha, t), y(\alpha, t)$ have smooth extensions across $\alpha = 0$ defined by $x(-\alpha, t) = -x(\alpha, t)$, $y(-\alpha, t) = y(\alpha, t)$, It follows that for $\alpha \approx 0$,

$$x(\alpha, t) = \dot{x}_0(t)\alpha + \frac{\dddot{x}_0(t)}{6}\alpha^3 + O(\alpha^5), \tag{39}$$

$$y(\alpha, t) = y_0(t) + \frac{\ddot{y}_0(t)}{2}\alpha^2 + O(\alpha^4), \tag{40}$$

$$\kappa(\alpha, t) = \kappa_0(t) + \frac{\ddot{\kappa}_0(t)}{2}\alpha^2 + O(\alpha^4). \tag{41}$$

Similar expansions hold for $x(\alpha_j, t)$, $y(\alpha_j, t)$, and $\kappa(\alpha_j, t)$. We expand the functions $M(x, x_j, \xi)$'s and $Q(x, x_j, \xi)$'s about the base point $\mathbf{p} = (\dot{x}_0\alpha, \dot{x}_0\alpha_j, 0)$.

For example,

$$
\begin{aligned}
M(x,x_j,\xi) = M(\mathbf{p}) &+ \frac{\partial M}{\partial x}(\mathbf{p})\Big(\frac{\ddot{x}_0(t)}{6}\,\alpha^3+\dots\Big) + \frac{\partial M}{\partial x_j}(\mathbf{p})(\frac{\ddot{x}_0(t)}{6}\,\alpha_j^3+\dots) \\
&+ \frac{\partial M}{\partial \xi}(\mathbf{p})\Big(\frac{\ddot{y}_0(t)}{2}(\alpha^2-\alpha_j^2)+\dots\Big) \\
&+ \frac{\partial^2 M}{\partial \xi^2}(\mathbf{p})\Big(\frac{\ddot{y}_0^2(t)}{8}(\alpha^2-\alpha_j^2)^2+\dots\Big) \\
&+ \frac{\partial^2 M}{\partial \xi \partial x}(\mathbf{p})\Big(\frac{\ddot{y}_0(t)\ddot{x}_0(t)}{12}(\alpha^2-\alpha_j^2)\alpha^3+\dots\Big)+\dots
\end{aligned}
\tag{42}
$$

and similarly for Q's functions. We also define $\eta = \alpha/\alpha_j$. We substitute all these expassions into the integrands G (21)-(22) to obtain their the approximations at the left boundary. The number of terms needed in the Taylor expansions is determined by the desired order of accuracy and the dependence of derivatives of M, Q on α_j. As we will see, for the 5th order quadrature rules we need 4th order approximations of G. Furthermore, one can confirm that all first derivatives of M behave as $O(1/\alpha_j)$, all second derivatives of M behave as $O(1/\alpha_j^2)$, and all kth derivatives behave as $O(1/\alpha_j^k)$. The behaviour of Q differs slightly, in that its kth derivatives behave as $O(1/\alpha_j^{k+1})$. As a results, for the approximation of Q_{11} for example we need 14 terms.

The results, obtained with Mathematica, are that

$$G^u = B^{l,us}(\alpha,\alpha_j,t) + O(\alpha^5,\alpha_j^5), \tag{43}$$
$$G^{vs} = B^{l,vs}(\alpha,\alpha_j,t) + O(\alpha^4,\alpha_j^4), \tag{44}$$
$$G^{ud} = B^{l,ud}(\alpha,\alpha_j,t) + O(\alpha^5,\alpha_j^5), \tag{45}$$
$$G^{vd} = B^{l,vd}(\alpha,\alpha_j,t) + O(\alpha^4,\alpha_j^4), \tag{46}$$

where

$$B^{l,us}(\alpha,\alpha_j,t) = \alpha_j^3 b_1^{l,us}(t) B_1^{us}(\eta), \tag{47}$$
$$B^{l,vs}(\alpha,\alpha_j,t) = \alpha_j^2 b_1^{l,vs}(t) B_1^{vs}(\eta), \tag{48}$$
$$B^{l,ud}(\alpha,\alpha_j,t) = \alpha_j b_1^{ud}(t) B_1^{us}(\eta) + \alpha_j^3 \sum_{k=2}^{6} b_k^{l,ud}(t) B_k^{ud}(\eta), \tag{49}$$
$$B^{l,vd}(\alpha,\alpha_j,t) = \alpha_j^2 \sum_{k=1}^{2} b_k^{l,vd}(t) B_k^{vd}(\eta). \tag{50}$$

The functions $b(t)$ and $B(\eta)$ are given in Appendix D. Figure 8 displays both the integrands $G(\alpha,\alpha_j,t)$ and their approximations $B^l(\alpha,\alpha_j,t)$. For small α_j, there is an accurate agreement of these functions around the left endpoint and the approximations capture the behaviour of G at that point. What is

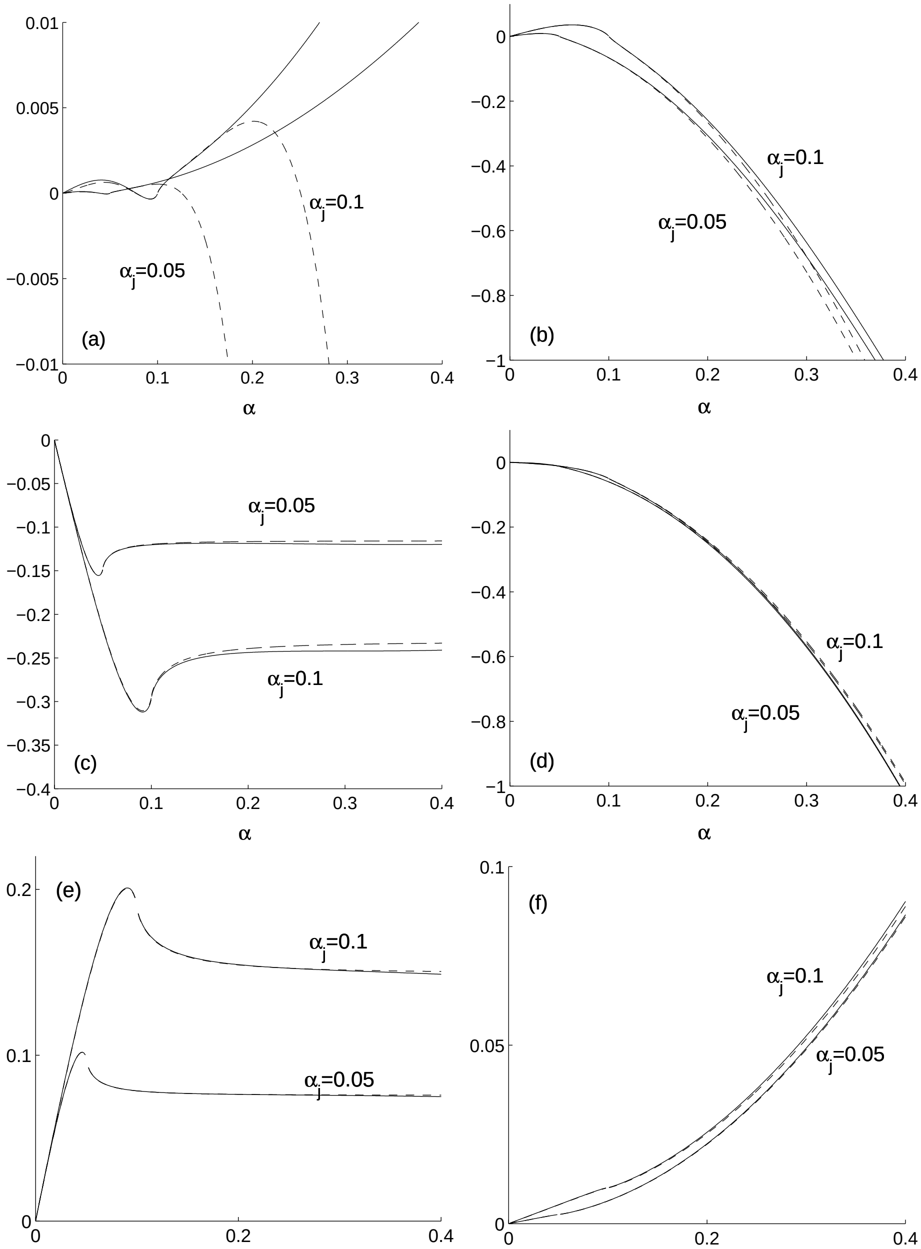

Fig. 6. Integrands $G^{\xi}(\alpha, \alpha_j, t)$ (solid lines) and their approximations $B^{l,\xi}(\alpha, \alpha_j, t)$ near the left endpoints $\alpha = \alpha_j = 0$ (dashed lines), shown for two values of $\alpha_j = 0.05$ and $\alpha_j = 0.1$. (a) $\xi = u_s$, (b) $\xi = v_s$, (c) and (d) $\xi = u_d$ and $\xi = v_d$, respectively, with u, v set to $\cos, \sin$, and (e) and (f) $\xi = u_d$ and $\xi = v_d$, respectively, u, v for $\lambda = 0$ computed iteratively.

notable from (47)-(50) is that the coefficients $b(t)$ are independent of j – they depend on derivatives of x, y, k, u, v at the endpoints – and the functions $B(\eta)$ are independent of time. Thus the integral of $B_k(\eta)$ can be precomputed at time $t = 0$ and the integrals of the approximation B can be computed at each timestep solely by computing the coefficients $b_k(t)$ at a cost of O(1).

For convenience, as will be explained shortly, we will integrate B over an interval proportional to α_j of the form $[0, L\alpha_j]$ where we choose $L = 10$ to be sufficiently large to cover the range in which B approximates G well. The procedure is as follows: extend B by 0 on $[10\alpha_j, \infty)$ and extend G by 0 on $[\pi, \infty)$. To compute $\int G d\alpha$ now write

$$\begin{aligned} \int_0^\pi G d\alpha &= \int_0^\infty G - B^l d\alpha + \int_0^\infty B^l d\alpha \\ &\approx T[G - B^l]^h_{[0,\infty)} + \int_0^\infty B^l d\alpha \\ &= T[G]^h_{[0,\pi]} + \left(\int_0^{10\alpha_j} B^l d\alpha - T[B^l]^h_{[0,10\alpha_j]} \right) \\ &= T[G]^h_{[0,\pi]} + E[B^l]^h_{[0,10\alpha_j]}. \end{aligned} \tag{51}$$

The numbers $E[B]$ are therefore local corrections to our original approximation. Since for any function $f(\alpha, \alpha_j, t)$, $E[f]^h_{[0,10\alpha_j]} = \alpha_j E[f]^{1/j}_{[0,10]}$ it follows that

$$E[B^{l,us}]^h_{[0,10\alpha_j]} = \alpha_j^4 b_1^{l,us}(t) E[B_1^{us}]^{1/j}_{[0,10]}, \tag{52}$$

$$E[B^{l,vs}]^h_{[0,10\alpha_j]} = \alpha_j^3 b_1^{l,vs}(t) E[B_1^{vs}]^{1/j}_{[0,10]}, \tag{53}$$

$$E[B^{l,ud}]^h_{[0,10\alpha_j]} = \alpha_j^2 b_1^{l,ud}(t) E[B_1^{ud}]^{1/j}_{[0,10]} + \alpha_j^4 \sum_{k=2}^{6} b_k^{l,ud}(t) E[B_k^{ud}]^{1/j}_{[0,10]}, \tag{54}$$

$$E[B^{l,vd}]^h_{[0,10\alpha_j]} = \alpha_j^3 \sum_{k=1}^{2} b_k^{l,vd}(t) E[B_k^{vd}]^{1/j}_{[0,10]}. \tag{55}$$

Here the time-independent factors $E[B_k^l]^{1/j}_{[0,10]}$ are precomputed at $t = 0$. Because the integration interval for B was chosen to be proportional to α_j, these factors are also independent of h and can be precomputed once for all meshes to be used. This explains the reason for the particular choice for integration interval for B.

Notice also that the form of the corrections (52)-(55) shows that near the left endpoint the maximum error in the original approximation $T[G]$ occurs when $\alpha_j = h$ (j=1) and that it is $O(h^4)$ for G^{us} $O(h^3)$ for G^{vs}, G^{vd}, and $O(h^2)$ for G^{ud}, in agreement with the numerical results in Fig. 8. Thus, this method yields second, third, and fourth order corrections to produce an approximation that is uniformly 5th order near the left endpoint.

Similarly, to obtain uniformity near the right endpoint we find an approximations of the integrands G near $\alpha, \alpha_j = \pi$, which turn out to be given by

$$B^{r,us}(\alpha, \alpha_j, t) = (\alpha_j - \pi)^3 b_1^{r,us}(t) B_1^{us}(\eta), \tag{56}$$
$$B^{r,vs}(\alpha, \alpha_j, t) = (\alpha_j - \pi)^2 b_1^{r,vs}(t) B_1^{vs}(\eta), \tag{57}$$
$$B^{r,ud}(\alpha, \alpha_j, t) = (\alpha_j - \pi) b_1^{ud}(t) B_1^{us}(\eta) + (\alpha_j - \pi)^3 \sum_{k=2}^{6} b_k^{r,ud}(t) B_k^{ud}(\eta), \tag{58}$$
$$B^{r,vd}(\alpha, \alpha_j, t) = (\alpha_j - \pi)^2 \sum_{k=1}^{2} b_k^{r,vd}(t) B_k^{vd}(\eta), \tag{59}$$

where $\eta = (\alpha - \pi)/(\alpha_j - \pi)$ and the coefficients b^r have the same form as the coefficients b^l given in Appendix D except that all subscripts 0 are replaced by the subscripts n.

The final approximation we use is:

$$\int_0^\pi G\, d\alpha \approx Q[G] = T[G]^h_{[0,\pi]} + w_1(\alpha_j) E[B^l]^h_{[0,10\alpha_j]} + w_2(\alpha_j) E[B^r]^h_{[\pi-10\alpha_j,\pi]} \tag{4.8}$$

where the weights w_1 and w_2 are positive functions that add up to one, vanish at one or the other end-point sufficiently fast, and are smooth and periodic. We choose $w_1 = \cos^8(\frac{\alpha_j}{2})/(\sin^8(\frac{\alpha_j}{2}) + \cos^8(\frac{\alpha_j}{2}))$ and $w_2 = \sin^8(\frac{\alpha_j}{2})/(\sin^8(\frac{\alpha_j}{2}) + \cos^8(\frac{\alpha_j}{2}))$.

All coefficients the c_k, the values $\widetilde{B}_k(\alpha_j, \alpha_j, t)$, and the derivatives of B_k needed to compute $E[B_k]$ are given in Appendix E. The numbers $E[B_k]^{1/j}$ are computed in quadruple precision to reduce the effect of roundoff error. The time-dependent constants $b_k^l(t)$, $b_k^r(t)$ depend on derivatives of x, y, κ, u, v at the endpoints that are computed spectrally.

The resulting approximation error after including the corrections

$$E^Q[G]^h_{[0,\pi]} = \int_0^\pi G\, d\alpha - Q[G], \tag{60}$$

is plotted in Fig. fig:uniform. Observe that the large errors near the poles have been eliminated. To confirm that the approximation is now uniformly 5th order, We plot in Fig. 8 the maximal error as a function of h on a loglog scale ($\times$) together with a line representing the function $y = Ch^5$. The good agreement between the data and the line away from the region dominated by roundoff error confirms that the method is uniformly 5th order.

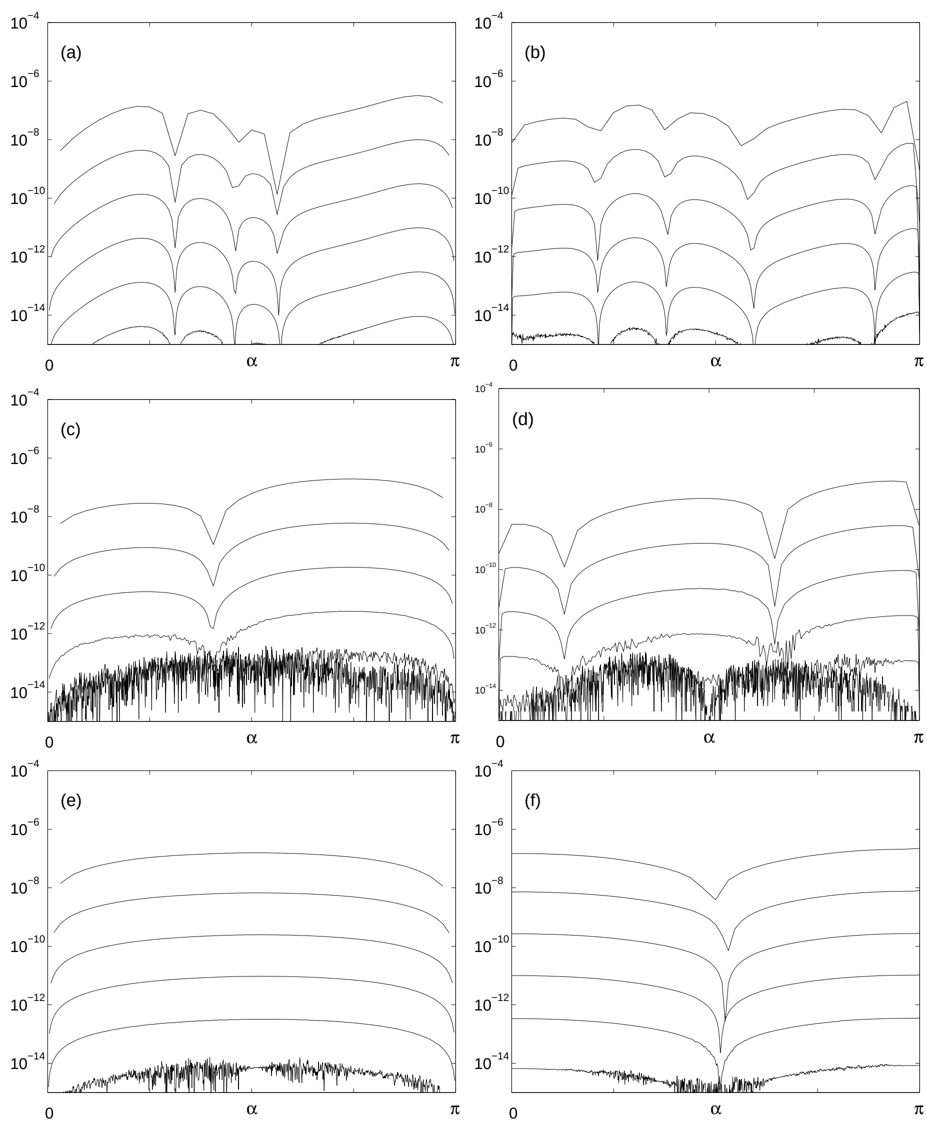

Fig. 7. Approximation error $E[G]^h_{[0,\pi]}$ using uniform 5th order method, including the correction for roundoff error. The values of h are $h = \pi/n$ with $n = 32$, 64, 128, 256, 512, 1024, for G equal to: (a) and (b), G^{us} and G^{vs}, respectively. (c) and (d), G^{ud} and G^{vd}, respectively, replacing u, v by $\sin\alpha, \cos\alpha$. (e) and (f), G^{ud} and G^{vd}, respectively, with u, v for $\lambda = 0$ obtained iteratively.

5 Concluding remarks

We presented uniformly 5th order accurate quadratures for the evaluation of the interfacial velocity in axi-symmetric Stokes flows. The proposed quadratures are based on an asymptotic analysis of the singular integrands, application of a modified Euler-Maclaurin formula, and the use of local pole corrections. The new quadratures have little overhead and can thus achieve a desired high level of accuracy for a fraction of the cost of commonly used second order approximations.

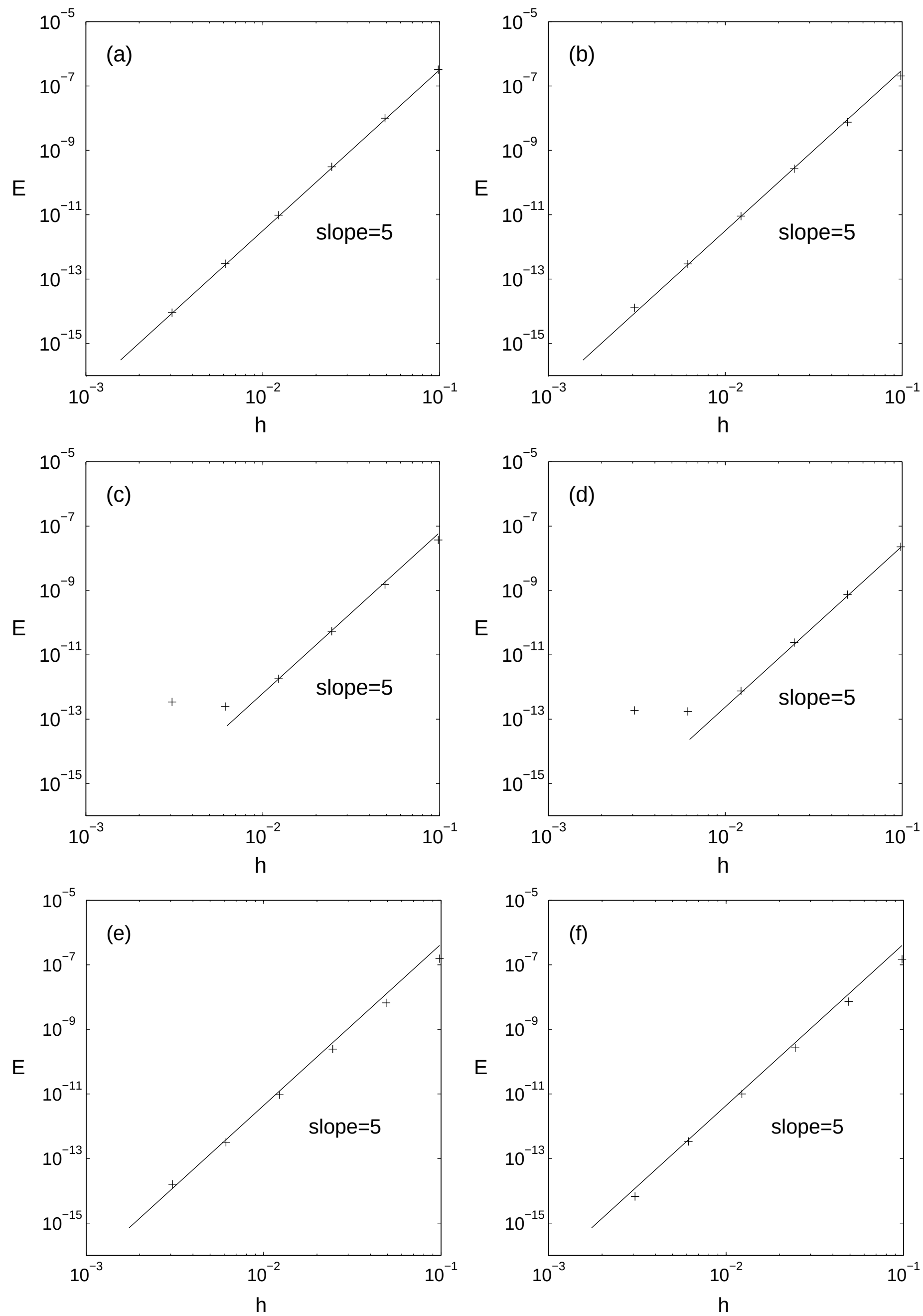

Fig. 8. Maximal Approximation error $\max_{\alpha_j \in [0,\pi/2]} \left(E[G]^h_{[0,\pi]}(\alpha_j) \right)$ using uniform 5th order method, for G equal to: (a) and (b), G^{us} and G^{vs}, respectively. (c) and (d), G^{ud} and G^{vd}, respectively, replacing u, v by $\sin\alpha, \cos\alpha$. (e) and (f), G^{ud} and G^{vd}, respectively, with u, v for $\lambda = 0$ obtained iteratively. The data is shown by $\times$, and the slope of the plotted lines indicates the estimated order of the approximation.

We have focused here on the case of a single drop but the quadratures can also be applied to multiple drops. It merely requires a combination of the modified trapezoidal rule of 5th order for the regular boundary integrals (introduced by the presence of other drops) and our proposed quadratures.

It is also possible to introduce adaptivity by suitably controlling the parametrization of the interface or interfaces. For example one can cluster nodes on the interface around a coalescence or break up region by this simple change of variables. This procedure does not change at all the application of the proposed quadratures.

6 Acknowledgments

H.D.C. acknowledges partial support for this research by the National Science Foundation through Grant DMS 0311911. M.N. acknowledges the support of the National Science Foundation through Grant DMS-0308061.

A Functions M and Q

$$
\begin{aligned}
M_1^u(x, x_j, \xi) &= x[I_{11} + (x^2 + x_j^2)I_{31} - xx_j(I_{30} + I_{32})], && \text{(A.1)}\\
M_2^u(x, x_j, \xi) &= x\xi(xI_{31} - x_j I_{30}), && \text{(A.2)}\\
M_1^v(x, x_j, \xi) &= x\xi(xI_{30} - x_j I_{31}), && \text{(A.3)}\\
M_2^v(x, x_j, \xi) &= x(I_{10} + \xi^2 I_{30}), && \text{(A.4)}\\
& && \text{(A.5)}
\end{aligned}
$$

$$
\begin{aligned}
Q_{11}^u(x, x_j, \xi) &= -6x[x^3 I_{51} - x^2 x_j (I_{50} + 2I_{52}) \\
&\qquad + xx_j^2(I_{53} + 2I_{51}) - x_j^3 I_{52}], && \text{(A.6)}\\
Q_{12}^u(x, x_j, \xi) &= -6x\xi[(x^2 + x_j^2)I_{51} - xx_j(I_{50} + I_{52})], && \text{(A.7)}\\
Q_{21}^u(x, x_j, \xi) &= Q_{12}^u, && \text{(A.8)}\\
Q_{22}^u(x, x_j, \xi) &= -6x\xi^2(xI_{51} - x_j I_{50}), && \text{(A.9)}\\
Q_{11}^v(x, x_j, \xi) &= -6x\xi(x_j^2 I_{52} + x^2 I_{50} - 2xx_j I_{51}), && \text{(A.10)}\\
Q_{12}^v(x, x_j, \xi) &= -6x\xi^2(xI_{50} - x_j I_{51}), && \text{(A.11)}\\
Q_{21}^v(x, x_j, \xi) &= Q_{12}^v(x, x_j, \xi), && \text{(A.12)}\\
Q_{22}^v(x, x_j, \xi) &= -6x\xi^3 I_{50}, && \text{(A.13)}
\end{aligned}
$$

with

$$I_{10} = \frac{4}{c}F(k), \tag{A.14}$$

$$I_{11} = \frac{4}{c}a[bF(k) - E(k)], \tag{A.15}$$

$$I_{30} = \frac{4}{c^3}E_{3/2}(k), \tag{A.16}$$

$$I_{31} = \frac{4}{c^3}a[bE_{3/2}(k) - F(k)], \tag{A.17}$$

$$I_{32} = \frac{4}{c^3}a^2[b^2E_{3/2}(k) - 2bF(k) + E(k)], \tag{A.18}$$

$$I_{50} = \frac{4}{c^5}E_{5/2}(k), \tag{A.19}$$

$$I_{51} = \frac{4}{c^5}a[bE_{5/2}(k) - E_{3/2}(k)], \tag{A.20}$$

$$I_{52} = \frac{4}{c^5}a^2[b^2E_{5/2}(k) - 2bE_{3/2}(k) + F(k)], \tag{A.21}$$

$$I_{53} = \frac{4}{c^5}a^3[b^3E_{5/2}(k) - 3b^2E_{3/2}(k) + 3bF(k) - E(k)], \tag{A.22}$$

where

$$k^2 = \frac{4xx_j}{\xi^2 + (x + x_j)^2}, \tag{A.23}$$

and $a = 2/k^2$, $b = (2 - k^2)/2$, $c^2 = (x + x_j)^2 + \xi^2$. Here, F and E are the complete elliptic integrals of the first and second kind, respectively:

$$F(k) = \int_0^{\pi/2} \frac{d\theta}{\sqrt{1 - k^2 \sin^2\theta}} , \quad E(k) = \int_0^{\pi/2} \sqrt{1 - k^2 \sin^2\theta}d\theta , \tag{A.24}$$

and

$$E_{3/2} = \frac{E(k)}{1 - k^2} , \quad E_{5/2}(k) = \frac{2(2 - k^2)}{3(1 - k^2)^2}E(k) - \frac{F(k)}{3(1 - k^2)} . \tag{A.25}$$

Notice that a and b are functions of k only, with $a \to 2$ and $b \to 1/2$ as $k \to 1$. Using this formulations of I_{jk} (which differs from slightly from the formulations in [14]) it is easy to see that the most singular contributions to I_{3j} and I_{5j} at $k = 1$, which comes from the $E_{3/2}$ and the $E_{5/2}$ terms, respectively, are

$$I_{3j} \sim \frac{4}{c^3}\frac{1}{1 - k^2} \quad , I_{5j} \sim \frac{4}{c^5}\frac{1}{(1 - k^2)^2}. \tag{A.26}$$

This fact is used in Section 3.2.

B Integrands for $\alpha_j = 0, \pi$

The integrands in (21)-(22) degenerate as $\alpha_j \to 0, \pi$ to smooth functions that can easily be integrated. Here we state these functions and all their values and derivatives at the endpoints needed to implement the quadrature rule (24). The limiting integrands are found by expanding M and Q about $x_j = 0$ using known expansions of $F(k)$ and $E(k)$ about $k = 0$. The integrands are denoted by G, i.e $G(\alpha, \alpha_j, t) = H(\alpha, \alpha_j, t)g(\alpha)$, where $g = \kappa$, u or v, as appropriate. The limiting functions are:

$$G^u_s(\alpha, \alpha_{jend}, t) = 0, \tag{B.1}$$

$$G^v_s(\alpha, \alpha_{jend}, t) = \frac{2\pi x\kappa}{(x^2+\xi^2)^{3/2}}[\dot{y}x\xi - \dot{x}(2\xi^2 + x^2)], \tag{B.2}$$

$$G^u_d(\alpha, \alpha_{jend}, t) = 0, \tag{B.3}$$

$$G^v_d(\alpha, \alpha_{jend}, t) = -\frac{12\pi x\xi}{(x^2+\xi^2)^{5/2}}(ux + v\xi)(x\dot{y} - \xi\dot{x}), \tag{B.4}$$

where $jend = 0$ or n, and $x = x(\alpha), y = y(\alpha), \xi = y(\alpha) - y_{jend}$. To integrate these functions with the modified trapezoid rule we need their limiting value at $\alpha = \alpha_{jend}$ and their first and third derivatives at the endpoints. At the left endpoint, $\alpha_{jend} = 0$, they are :

$$G^v_s(0, 0, t) = -2\pi\kappa_0|\dot{x}_0|, \tag{B.5}$$

$$\frac{d}{d\alpha}G^v_d(0, 0, t) = 0, \tag{B.6}$$

$$\frac{d^3}{d^3\alpha}G^v_d(0, 0, t) = 0, \tag{B.7}$$

$$\frac{d}{d\alpha}G^v_s(\pi, 0, t) = -\frac{4\pi\kappa_n\dot{x}_n^2}{|\xi|} \tag{B.8}$$

$$\frac{d^3}{d\alpha^3}G^v_s(\pi, 0, t) = -\frac{4\pi\dot{x}_n}{|\xi|^3}\Big[3\ddot{\kappa}_n\dot{x}_n\xi^2 - \kappa_n\Big(6\dot{x}_n^3 - 4\dddot{x}_n\xi^2 + 6\dot{x}_n\xi\ddot{y}_n\Big)\Big], \tag{B.9}$$

$$G^v_d(0, 0, t) = 0, \tag{B.10}$$

$$\frac{d}{d\alpha}G^v_d(0, 0, t) = 0, \tag{B.11}$$

$$\frac{d^3}{d^3\alpha}G^v_d(0, 0, t) = 0, \tag{B.12}$$

$$\frac{d}{d\alpha}G^v_d(\pi, 0, t) = \frac{12\pi v_n\dot{x}_n^2}{\xi|\xi|}, \tag{B.13}$$

$$\begin{aligned}\frac{d^3}{d\alpha^3}G^v_d(\pi, 0, t) = \frac{12\pi\dot{x}_n}{\xi^3|\xi|}&\Big[3\dot{x}_n\xi\Big(2\dot{u}_n\dot{x}_n + \ddot{v}_n\xi\Big)\\ &- v_n\Big(15\dot{x}_n^3 - 4\dddot{x}_n\xi^2 + 12\dot{x}_n\xi\ddot{y}_n\Big)\Big],\end{aligned} \tag{B.14}$$

where $\xi = y_n - y_0$. At the right endpoint, $\alpha_{jend} = \pi$, they are :

$$
\begin{aligned}
G_s^v(\pi,\pi,t) &= 2\pi\kappa_n|\dot{x}_n|, && \text{(B.15)}\\
\frac{d}{d\alpha}G_s^v(\pi,\pi,t) &= 0, && \text{(B.16)}\\
\frac{d^3}{d^3\alpha}G_s^v(\pi,\pi,t) &= 0, && \text{(B.17)}\\
\frac{d}{d\alpha}G_s^v(0,\pi,t) &= -\frac{4\pi\kappa_0\dot{x}_0^2}{|\xi|}, && \text{(B.18)}\\
\frac{d^3}{d\alpha^3}G_s^v(0,\pi,t) &= \frac{4\pi\dot{x}_0}{|\xi|^3}\Big[-3\ddot{\kappa}_0\dot{x}_0\xi^2 + \kappa_0\Big(6\dot{x}_0^3 - 4\dddot{x}_0\xi^2 - 6\dot{x}_0\xi\ddot{y}_0\Big)\Big], && \text{(B.19)}\\
G_d^v(\pi,\pi,t) &= 0, && \text{(B.20)}\\
\frac{d}{d\alpha}G_d^v(\pi,\pi,t) &= 0, && \text{(B.21)}\\
\frac{d^3}{d^3\alpha}G_d^v(\pi,\pi,t) &= 0, && \text{(B.22)}\\
\frac{d}{d\alpha}G_d^v(0,\pi,t) &= -\frac{12\pi v_0\xi\dot{x}_0^2}{|\xi|^3}, && \text{(B.23)}\\
\frac{d^3}{d\alpha^3}G_d^v(0,\pi,t) &= \frac{12\pi\dot{x}_0}{\xi^3|\xi|}\Big[3\dot{x}_0\xi\Big(2\dot{u}_0\dot{x}_0 - \ddot{v}_0\xi\Big) \\
&\quad + v_0\Big(15\dot{x}_0^3 - 4\dddot{x}_0\xi^2 - 12\dot{x}_0\xi\ddot{y}_0\Big)\Big], && \text{(B.24)}
\end{aligned}
$$

where, as above, $\xi = y_n - y_0$.

C Relevant coefficients of $G(\alpha, \alpha_j, t)$

This appendix lists all the coefficients c_k of G and its derivatives at the endpoints needed to implement the pointwise quadrature (24). For $G^{u,s}(\alpha, \alpha_j, t)$, $\alpha_j \neq 0, \pi$, the values are:

$$
\begin{aligned}
\widetilde{G}^{u,s}(\alpha_j,\alpha_j,0) &= 0, && \text{(C.1)}\\
c_2^{u,s} &= -\ddot{\kappa}_j\dot{y}_j - \frac{2\dot{\kappa}_j}{x_j}(\dot{x}_j\dot{y}_j + \ddot{y}_j x_j), && \text{(C.2)}\\
\frac{dG^{u,s}}{d\alpha}(0,\alpha_j,t) &= \frac{2\pi(\kappa_0-\kappa_j)\dot{x}_0^2 x_j\xi}{[x_j^2+\xi^2]^{3/2}}\ ,\quad \xi = y_0 - y_j, && \text{(C.3)}\\
\frac{dG^{u,s}}{d\alpha}(\pi,\alpha_j,t) &= \frac{2\pi(\kappa_n-\kappa_j)\dot{x}_n^2 x_j\xi}{[x_j^2+\xi^2]^{3/2}}\ ,\quad \xi = y_n - y_j, && \text{(C.4)}
\end{aligned}
$$

$$
\begin{aligned}
\frac{d^3G^{u,s}}{d\alpha^3}(0,\alpha_j,t) = \frac{\pi\dot{x}_0 x_j}{[x_j^2+\xi^2]^{7/2}}\Big[&(\kappa_0-\kappa_j)\Big[12\dot{x}_0\ddot{y}_0(x_j^4-x_j^2\xi^2-2\xi^4) \\
&+ 9\dot{x}_0^3(x_j^2-4\xi^2)\xi + 8\dddot{x}_0(x_j^2+\xi^2)^2\xi\Big] \\
&+ 6\ddot{\kappa}_0\dot{x}_0(x_j^2+\xi^2)^2\xi\Big]\,, \quad \xi = y_0 - y_j,
\end{aligned} \tag{C.5}
$$

$$
\begin{aligned}
\frac{d^3G^{u,s}}{d\alpha^3}(\pi,\alpha_j,t) = \frac{\pi\dot{x}_n x_j}{[x_j^2+\xi^2]^{7/2}}\Big[&(\kappa_n-\kappa_j)\Big[12\dot{x}_n\ddot{y}_n(x_j^4-x_j^2\xi^2-2\xi^4) \\
&+ 9\dot{x}_n^3(x_j^2-4\xi^2)\xi + 8\dddot{x}_n(x_j^2+\xi^2)^2\xi\Big] \\
&+ 6\ddot{\kappa}_n\dot{x}_n(x_j^2+\xi^2)^2\xi\Big], \quad \xi = y_n - y_j,
\end{aligned} \tag{C.6}
$$

For $G^{v,s}$, $\alpha_j \neq 0, \pi$, the values are :

$$
\widetilde{G}^{v,s}(\alpha_j,\alpha_j,0) = 0, \tag{C.7}
$$

$$
c_2^{v,s} = \ddot{\kappa}_j\dot{x}_j + \frac{\dot{\kappa}_j}{x_j}(\dot{x}_j^2 + 2x_j\ddot{x}_j - \dot{y}_j^2), \tag{C.8}
$$

$$
\frac{dG^{v,s}}{d\alpha}(0,\alpha_j,t) = -\frac{2\pi(\kappa_0-\kappa_j)\dot{x}_0^2(x_j^2+2\xi^2)}{[x_j^2+\xi^2]^{3/2}},\ \xi = y_0 - y_j, \tag{C.9}
$$

$$
\frac{dG^{v,s}}{d\alpha}(\pi,\alpha_j,t) = -\frac{2\pi(\kappa_n-\kappa_j)\dot{x}_n^2(x_j^2+2\xi^2)}{[x_j^2+\xi^2]^{3/2}},\ \xi = y_n - y_j, \tag{C.10}
$$

$$
\begin{aligned}
\frac{d^3G^{v,s}}{d\alpha^3}(0,\alpha_j,t) = \frac{\pi\dot{x}_0}{[x_j^2+\xi^2]^{7/2}}\Big[&(\kappa_0-\kappa_j)\Big[-8\dddot{x}_0(x_j^2+\xi^2)^2(x_j^2+2\xi^2) \\
&- 3\dot{x}_0^3(x_j^4+8x_j^2\xi^2-8\xi^4) \\
&+ 12\dot{x}_0\ddot{y}_0(-x_j^4+x_j^2\xi^2+2\xi^4)\xi\Big] \\
&- 6\ddot{\kappa}_0\dot{x}_0(x_j^2+\xi^2)^2(x_j^2+2\xi^2)\Big]\,, \quad \xi = y_0 - y_j,
\end{aligned} \tag{C.11}
$$

$$
\begin{aligned}
\frac{d^3G^{v,s}}{d\alpha^3}(\pi,\alpha_j,t) = \frac{\pi\dot{x}_n}{[x_j^2+\xi^2]^{7/2}}\Big[&(\kappa_n-\kappa_j)\Big[-8\dddot{x}_n(x_j^2+\xi^2)^2(x_j^2+2\xi^2) \\
&- 3\dot{x}_n^3(x_j^4+8x_j^2\xi^2-8\xi^4) \\
&+ 12\dot{x}_n\ddot{y}_n(-x_j^4+x_j^2\xi^2+2\xi^4)\xi\Big] \\
&- 6\ddot{\kappa}_n\dot{x}_n(x_j^2+\xi^2)^2(x_j^2+2\xi^2)\Big]\,, \quad \xi = y_n - y_j,
\end{aligned} \tag{C.12}
$$

For $G^{u,d}$, $\alpha_j \neq 0, \pi$, the values are :

$$\widetilde{G}^{u,d}(\alpha_j,\alpha_j,0) = \frac{-2v_j\dot{x}_j\dot{y}_j(\dot{y}_j(\dot{x}_j^2+\dot{y}_j^2)-2x_j(\ddot{x}_j\dot{y}_j-\dot{x}_j\ddot{y}_j)}{x_j(\dot{x}_j^2+\dot{y}_j^2)^2} \tag{C.13}$$

$$+\frac{2u_j(\dot{y}_j(2\dot{x}_j^4+3\dot{y}_j^4)+\dot{x}_j^2\dot{y}_j(2x_j\ddot{x}_j+5\dot{y}_j^2)-2x_j\dot{x}_j^3\ddot{y}_j)}{x_j(\dot{x}_j^2+\dot{y}_j^2)^2} \tag{C.14}$$

$$c_2^{u,d} = -\frac{3\dot{v}_j\dot{y}_j^2}{x_j^2}, \tag{C.15}$$

$$\frac{dG^{u,d}}{d\alpha}(0,\alpha_j,t) = \frac{-12\pi(v_0-v_j)\dot{x}_0^2\xi^2x_j}{(x_j^2+\xi^2)^{5/2}}\ , \quad \xi = y_j - y_0, \tag{C.16}$$

$$\frac{dG^{u,d}}{d\alpha}(\pi,\alpha_j,t) = \frac{-12\pi(v_n-v_j)\dot{x}_n^2\xi^2x_j}{(x_j^2+\xi^2)^{5/2}}\ , \quad \xi = y_j - y_n, \tag{C.17}$$

$$\begin{aligned}\frac{d^3G^{u,d}}{d\alpha^3}(0,\alpha_j,t) = {}& \frac{6\pi x_j\dot{x}_0}{(x_j^2+\xi^2)^5}\Big[2\Big(3x_j^2\dot{u}_0\ddot{y}_0-\xi^2(3\dot{x}_0\ddot{v}_0+4\dddot{x}_0\Delta v)\Big)\\ &+\frac{6\dot{x}_0\xi(2x_j^2-3\xi^2)}{x_j^2+\xi^2}(\dot{x}_0\dot{u}_0-2\Delta v\ddot{y}_0)\\ &+\frac{15\dot{x}_0^3\xi^2\Delta v}{(x_j^2+\xi^2)^2}\Big(-3x_j^2+4\xi^2)\Big]\\ &\xi = y_0-y_j\ , \quad \Delta v = v_0 - v_j,\end{aligned} \tag{C.18}$$

$$\begin{aligned}\frac{d^3G^{u,d}}{d\alpha^3}(\pi,\alpha_j,t) = {}& \frac{6\pi x_j\dot{x}_n}{(x_j^2+\xi^2)^5}\Big[2\Big(3x_j^2\dot{u}_n\ddot{y}_n-\xi^2(3\dot{x}_n\ddot{v}_n+4\dddot{x}_n\Delta v)\Big)\\ &+\frac{6\dot{x}_n\xi(2x_j^2-3\xi^2)}{x_j^2+\xi^2}(\dot{x}_n\dot{u}_n-2\Delta v\ddot{y}_n)\\ &+\frac{15\dot{x}_n^3\xi^2\Delta v}{(x_j^2+\xi^2)^2}\Big(-3x_j^2+4\xi^2)\Big]\\ &\xi = y_n-y_j\ , \quad \Delta v = v_n - v_j.\end{aligned} \tag{C.19}$$

For $G^{v,d}$, $\alpha_j \neq 0, \pi$, the values are :

$$\widetilde{G}^{v,d}(\alpha_j, \alpha_j, 0) = \frac{-2\dot{y}_j(u_j\dot{x}_j + v_j\dot{y}_j)(\dot{x}_j^2\dot{y}_j - 2x_j\ddot{x}_j\dot{y}_j + \dot{y}_j^3 + 2x_j\dot{x}_j\ddot{y}_j)}{x_j(\dot{x}_j^2 + \dot{y}_j^2)^2}, \tag{C.20}$$

$$c_2^{v,d} = \frac{3\dot{u}_j\dot{y}_j^2}{x_j^2}, \tag{C.21}$$

$$\frac{dG^{v,d}}{d\alpha}(0, \alpha_j, t) = \frac{12\pi(v_0 - v_j)\dot{x}_0^2\xi^3}{(x_j^2 + \xi^2)^{5/2}}\ , \quad \xi = y_j - y_0, \tag{C.22}$$

$$\frac{dG^{v,d}}{d\alpha}(\pi, \alpha_j, t) = \frac{12\pi(v_n - v_j)\dot{x}_n^2\xi^3}{(x_j^2 + \xi^2)^{5/2}}\ , \quad \xi = y_j - y_n, \tag{C.23}$$

$$\begin{aligned} \frac{d^3G^{v,d}}{d\alpha^3}(0, \alpha_j, t) = {} & \frac{6\pi\xi\dot{x}_0}{(x_j^2 + \xi^2)^5}\Big[2\Big(- 3x_j^2\dot{u}_0\ddot{y}_0 + \xi^2(3\dot{x}_0\ddot{v}_0 + 4\dddot{x}_0\Delta v)\Big) \\ & + \frac{6\dot{x}_0\xi(3x_j^2 - 2\xi^2)}{x_j^2 + \xi^2}(-\dot{x}_0\dot{u}_0 + 2\Delta v\ddot{y}_0) \\ & + \frac{15\dot{x}_0^3\xi^2\Delta v}{(x_j^2 + \xi^2)^2}\Big(5x_j^2 - 2\xi^2\Big)\Big] \\ & \xi = y_0 - y_j\ , \quad \Delta v = v_0 - v_j, \end{aligned} \tag{C.24}$$

$$\begin{aligned} \frac{d^3G^{v,d}}{d\alpha^3}(\pi, \alpha_j, t) = {} & \frac{6\pi\xi\dot{x}_n}{(x_j^2 + \xi^2)^5}\Big[2\Big(- 3x_j^2\dot{u}_n\ddot{y}_n + \xi^2(3\dot{x}_n\ddot{v}_n + 4\dddot{x}_n\Delta v)\Big) \\ & + \frac{6\dot{x}_n\xi(3x_j^2 - 2\xi^2)}{x_j^2 + \xi^2}(-\dot{x}_n\dot{u}_n + 2\Delta v\ddot{y}_n) \\ & + \frac{15\dot{x}_n^3\xi^2\Delta v}{(x_j^2 + \xi^2)^2}\Big(5x_j^2 - 2\xi^2\Big)\Big] \\ & \xi = y_n - y_j\ , \quad \Delta v = v_n - v_j. \end{aligned} \tag{C.25}$$

For $\alpha_j = 0, \pi$ the function $G_s^u(\alpha, \alpha_j, t) = 0$. The function $G_s^v(\alpha, \alpha_j, t)$ given by (19) is smooth, so $c_0 = c_2 = 0$ and $\widetilde{G}_s^v(\alpha_j, \alpha_j, t) = G_s^v(\alpha_j, \alpha_j, t)$. For $\alpha_j = 0$, the derivatives at the endpoints are:

$$G_s^{v\prime}(0,0,t) = 0, \tag{C.26}$$
$$G_s^{v\prime\prime\prime}(0,0,t) = 0, \tag{C.27}$$
$$G_s^{v\prime}(\pi,0,t) = -\frac{4\pi\kappa_n\dot{x}_n^2}{|y_0-y_n|}, \tag{C.28}$$
$$\begin{aligned} G_s^{v\prime\prime\prime}(\pi,0,t) = \frac{4\pi\dot{x}_n}{|y_n-y_0|^3}\Big[&-3\ddot{\kappa}_n\dot{x}_n(y_0-y_n)^2 \\ &+\kappa_n\Big(6\dot{x}_n^3-4\dddot{x}_n(y_0-y_n)^2-6\dot{x}_n\ddot{y}_n(y_0-y_n).\Big)\Big] \end{aligned} \tag{C.29}$$

For $\alpha_j = \pi$, the derivatives at the endpoints are

$$G_s^{v\prime}(\pi,\pi,t) = 0, \tag{C.30}$$
$$G_s^{v\prime\prime\prime}(\pi,\pi,t) = 0, \tag{C.31}$$
$$G_s^{v\prime}(0,\pi,t) = -\frac{4\pi\kappa_0\dot{x}_0^2}{|y_0-y_n|}, \tag{C.32}$$
$$\begin{aligned} G_s^{v\prime\prime\prime}(0,\pi,t) = \frac{4\pi\dot{x}_0}{|y_0-y_n|^3}\Big[&-3\ddot{\kappa}_0\dot{x}_0(y_0-y_n)^2 \\ &+\kappa_0\Big(6\dot{x}_0^3-4\dddot{x}_0(y_0-y_n)^2+6\dot{x}_0\ddot{y}_0(y_0-y_n). \end{aligned} \tag{C.33}$$

D Approximating functions $B(\alpha, \alpha_j, t)$

This appendix contains all the approximations of G to 5th order near the poles, i.e, $G = B(\alpha,\alpha_j,t) + O(\alpha^5,\alpha_j^5)$ where B is as given below. Throughout it, $\eta = \alpha/\alpha_j$ and $k^2 = 4\eta/(1+\eta)^2$.

$$B^{l,us}(\alpha,\alpha_j,t) = \alpha_j^3 b_1^{us}(t) B_1^{us}(\eta), \tag{D.1}$$
$$b_1^u(t) = \frac{\ddot{\kappa}_0\dot{x}_0\ddot{y}_0}{|\dot{x}_0|}, \tag{D.2}$$
$$B_1^{us}(\eta) = \frac{\eta}{2}(1-\eta^2)\Big[3(1+\eta)E(k) - \left(\frac{1+3\eta^2}{1+\eta}\right)F(k)\Big], \tag{D.3}$$

$$B^{l,vs}(\alpha,\alpha_j,t) = \alpha_j^2 b_1^{vs}(t) B_1^{vs}(\eta), \tag{D.4}$$
$$b_1^{vs}(t) = \frac{\ddot{\kappa}_0\dot{x}_0^2}{|\dot{x}_0|}, \tag{D.5}$$
$$B_1^{vs}(\eta) = -2\eta\frac{\eta^2-1}{1+\eta}F(k). \tag{D.6}$$

$$B^{ud}(\alpha,\alpha_j,t) = \alpha_j b_1^{ud}(t) B_1^{ud}(\eta) + \alpha_j^3 \sum_{k=2}^{6} b_k^{ud}(t) B_k^{ud}(\eta), \tag{D.7}$$

$$b_1^{ud}(t) = \frac{v_0 \ddot{y}_0^2}{\dot{x}_0 |\dot{x}_0|}, \tag{D.8}$$

$$B_1^{ud}(\eta) = -3\eta \Big[(1+\eta)E(k) + (1-\eta)F(k)\Big], \tag{D.9}$$

$$b_2^{ud}(t) = \frac{\dot{u}_0}{\dot{x}_0|\dot{x}_0|}\left[\frac{4}{3}\dddot{x}_0\ddot{y}_0 + \frac{5}{2}\frac{\ddot{y}_0^3}{\dot{x}_0} - \frac{1}{3}\ddddot{y}_0\dot{x}_0\right], \tag{D.10}$$

$$B_2^{ud}(\eta) = \eta(1+\eta)\Big[(1+\eta^2)E(k) - (1-\eta)^2 F(k)\Big], \tag{D.11}$$

$$b_3^{ud}(t) = \frac{v_0 \dddot{x}_0 \ddot{y}_0^2}{\dot{x}_0^2|\dot{x}_0|}, \tag{D.12}$$

$$B_3^{ud}(\eta) = \frac{\eta}{6}\Big[(1+\eta)(23+5\eta^2)E(k) + (1-\eta)(1+5\eta^2)F(k)\Big], \tag{D.13}$$

$$b_4^{ud}(t) = \frac{v_0 \ddot{y}_0 \ddddot{y}_0}{\dot{x}_0|\dot{x}_0|}, \tag{D.14}$$

$$B_4^{ud}(\eta) = -\frac{\eta}{6}\Big[5(1+\eta+\eta^2+\eta^3)E(k) + (1-\eta)(1+5\eta^2)F(k)\Big], \tag{D.15}$$

$$b_5^{ud}(t) = \frac{\ddot{v}_0 \ddot{y}_0^2}{\dot{x}_0|\dot{x}_0|}, \tag{D.16}$$

$$B_5^{ud}(\eta) = -\frac{3\eta^3}{2}\Big[(1+\eta)E(k) + (1-\eta)F(k)\Big], \tag{D.17}$$

$$b_6^{ud}(t) = \frac{v_0 \ddot{y}_0^4}{\dot{x}_0^3|\dot{x}_0|}, \tag{D.18}$$

$$B_6^{ud}(\eta) = \frac{5}{8}\eta(1+\eta)\Big[(7+\eta^2)E(k) - (1-\eta)^2 F(k)\Big]. \tag{D.19}$$

$$B^{vd}(\alpha,\alpha_j,t) = \alpha_j^2 \sum_{k=1}^{2} b_k^{vd}(t) B_k^{vd}(\eta), \tag{D.20}$$

$$b_1^{vd}(t) = \frac{\dot{u}_0 \ddot{y}_0^2}{\dot{x}_0|\dot{x}_0|}, \tag{D.21}$$

$$B_1^{vd}(\eta) = -3\eta\Big[(1+\eta)E(k) + (\eta-1)F(k)\Big], \tag{D.22}$$

$$b_2^{vd}(t) = \frac{v_0 \ddot{y}_0^3}{\dot{x}_0^2|\dot{x}_0|}, \tag{D.23}$$

$$B_2^{vd}(\eta) = -3\eta(1+\eta)E(k). \tag{D.24}$$

E Relevant coefficients of $B_s^{u,v}$

The functions $B_k^{u/v,s/d}$ are all of the form

$$B_k(\eta) = \widetilde{B}_k(\eta) \sum_{l=0}^{\infty} c_{k,j}\ (\eta-1)^j \log|\eta-1|. \tag{E.1}$$

The coefficients and derivatives necessary to compute $E[B]$, as in (ref) are indexed by $u/v, s/d$ as appropriate. The results are obtained with Mathematica.All real numbers are rounded to as many digits as listed.

$$c_{1,0}^{u,s} = 0, \tag{E.2}$$
$$c_{1,2}^{u,s} = -5, \tag{E.3}$$
$$\widetilde{B}_1^{u,s}(1) = 0, \tag{E.4}$$
$$\frac{dB_1^{u,s}}{d\eta}(0) = \pi/2, \tag{E.5}$$
$$\frac{d^3 B_1^{u,s}}{d\eta^3}(0) = -27\pi/4, \tag{E.6}$$
$$\frac{dB_1^{u,s}}{d\eta}(10) = 15.70828565, \tag{E.7}$$
$$\frac{d^3 B_1^{u,s}}{d^3\eta}(10) = 0.00003929, \tag{E.8}$$

$$c_{1,0}^{v,s} = 0, \tag{E.9}$$
$$c_{1,2}^{v,s} = 2, \tag{E.10}$$
$$\widetilde{B}_1^{v,s}(1) = 0, \tag{E.11}$$
$$\frac{dB_1^{v,s}}{d\eta}(0) = \pi, \tag{E.12}$$
$$\frac{d^3 B_1^{v,s}}{d\eta^3}(0) = -9\pi/2, \tag{E.13}$$
$$\frac{dB_1^{v,s}}{d\eta^3}(10) = -62.8325457383, \tag{E.14}$$
$$\frac{d^3 B_1^{v,s}}{d\eta^3}(10) = -0.0000841112. \tag{E.15}$$

References

[1] A. Acrivos, The breakup of small drops and bubbles in shear flows, Ann. N.Y. Acad. Sci. 404 (1983) 1–11.

[2] A. Acrivos, The deformation of small viscous drops and bubbles in shear flows, Annu. Rev. Fluid Mech. 16 (1984) 45–66.

[3] H. Stone, L. G. Leal, Relaxation and breakup of an initially extended drop in an otherwise quiescent fluid, J. Fluid Mech. 198 (1989) 399–427.

[4] M. Manga, H. Stone, Buoyancy-driven interactions between deformable drops at low reynolds numbers, J. Fluid Mech. 256 (1993) 647–683.

[5] M. Loewenberg, E. J. Hinch, Numerical simulation of a concentrated emulsion in shear flow, J. Fluid Mech. 321 (1996) 395–419.

[6] A. Z. Zinchenko, M. A. Rother, R. H. Davis, A novel boundary integral algorithm for viscous interaction of deformable drops, Phys. Fluids 9 (1997) 1493–1511.

[7] V. Cristini, J. Blawzdziewich, M. Loewenberg, Drop breakup in three-dimensional viscous flows, Phys. Fluids 10 (1998) 1781–1783.

[8] R. H. Davis, Buoyancy-driven viscous interaction of a rising drop with a smaller trailing drop, Phys. Fluids 11 (5) (1999) 1016–1028.

[9] G. K. Youngren, A. Acrivos, On the shape of a gas bubble in a viscous extensional flow, J. Fluid Mech. 76 (1976) 433.

[10] C. Pozrikidis, Boundary Integral and Singularity Methods for Linearized Viscous Flow, Cambridge Univ. Press, Cambridge, U.K., 1992.

[11] C. Pozrikidis, Interfacial dynamics for Stokes flows, J. Comput. Phys. 169 (2) (2001) 250.

[12] M. Nitsche, Axisymmetric vortex sheet motion: accurate evaluation of the principal value integral, SIAM J. Sci. Comput. 21 (3) (1999) 1066–1084.

[13] A. Sidi, M. Israeli, Quadrature methods for periodic singular and weakly singular Fredholm integral equations, J. Sci. Comput. (1988) 67–91.

[14] S. H. Lee, L. G. Leal, The motion of a sphere in the presence of a deformable interface. II. A numerical study of a translation of a sphere normal to an interface, J. Colloid Interface 87 (1982) 81–106.

[15] G. R. Baker, D. I. Meiron, S. A. Orszag, Boundary integral methods for axisymmetric and three dimensional Rayleigh-Taylor instability problems, Physica D 12 (1984) 19–31.

[16] B. de Bernadinis, D. W. Moore, A ring-vortex representation of an axi-symmetric vortex shee, in: Studies of Vortex Dominated Flows, Springer, 1987, pp. 33–43.

[17] D. A. Pugh, Development of vortex sheets in Boussinesq flows–Formation of singularities, Ph.D. thesis, Imperial College of Science and Technology (1989).

[18] Q. Nie, G. Baker, Application of adaptive quadrature to axi-symmetric vortex sheet motion, J. Comp. Phys. 143 (1998) 49–69.

[19] H. D. Ceniceros, H. Si, Computation of axisymmetric suction flow through porous media in the presence of surface tension, J. Comput. Phys. 165 (2000) 237–260.